Supplementary Information

Dislocation-engineered piezo-catalytic water splitting in single-crystal $BaTiO_3$

Yan Zhang[a], Kaiyu Feng[a], Miao Song[a,*], Shan Xiang[a], Yan Zhao[a], Hanyu Gong[a], Fan Ni[b], Felix Dietrich[c], Lovro Fulanović[b], Fangping Zhuo[b,*], Gerd Buntkowsky[c], Till Frömling[a,d], Dou Zhang[a,*], Chris Bowen[e], Jürgen Rödel[b]

Affiliations:

[a]State Key Laboratory of Powder Metallurgy, Central South University, Changsha, Hunan 410083, China

[b]Department of Materials and Earth Sciences, Technical University of Darmstadt, 64287 Darmstadt, Germany

[c]Institute of Physical Chemistry, Technical University of Darmstadt, 64287 Darmstadt, Germany

[d]Fraunhofer IWKS, Fraunhofer Research Institution for Materials Recycling and Resource Strategies, Hanau, Germany

[e]Department of Mechanical Engineering, University of Bath, Bath BA2 7AY, UK

*Corresponding authors: Miao Song, Fangping Zhuo, Dou Zhang

This file includes:

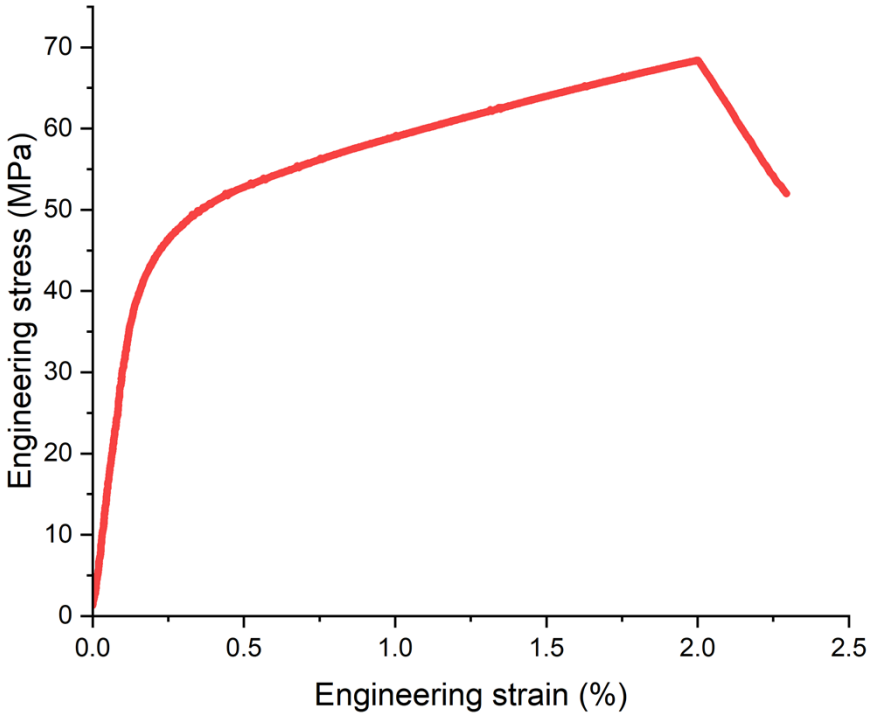

Fig. S1 High temperature uniaxial compressive deformation. Engineering stress-strain curves of the sample deformed at 1150 ℃ on loading along the [110] direction.

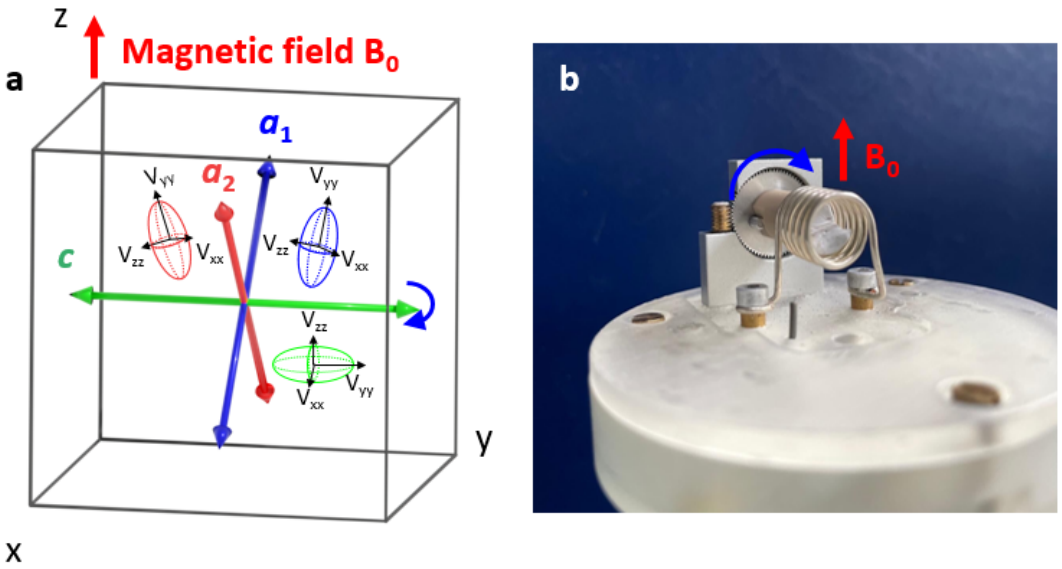

Fig. S2 Working principle for ^{137}Ba nuclear magnetic resonance (NMR) experiments. The orientations of the six spontaneous polarization vectors in a tetragonal phase are denoted by three distinct ellipsoids (blue, red, and green). These ellipsoids represent the orientation of the electric field gradient (EFG) tensor at the barium site, corresponding to different domain orientations (a_1, a_2, and c). b Photographic image of the sample holder for the NMR experiments. B_0 is the magnetic field along the z-axis.

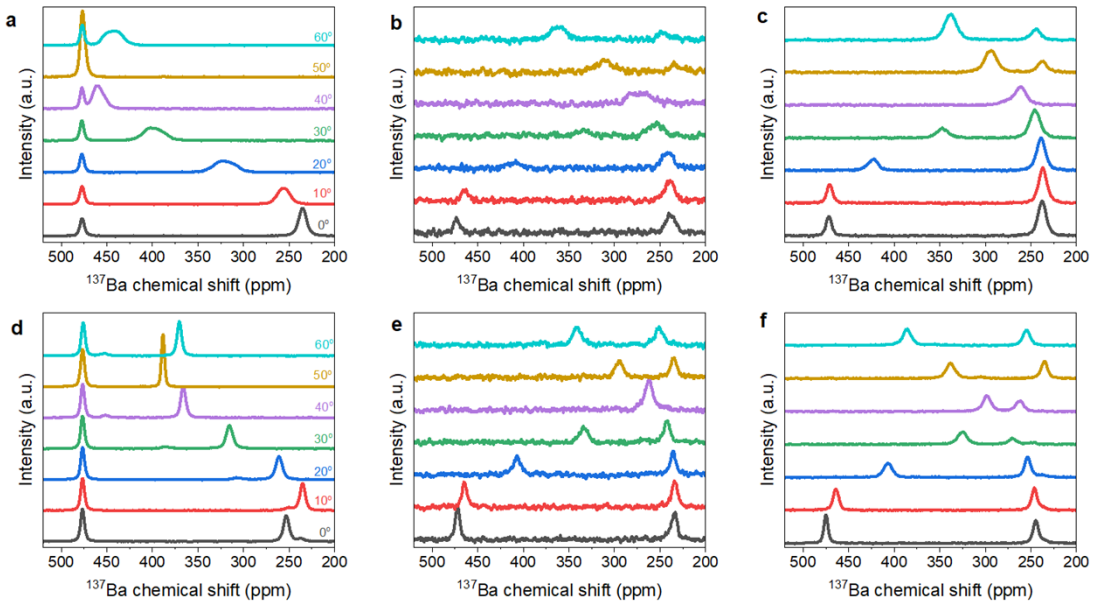

Fig. S3 Determination of domain configurations of both reference and deformed samples by ^{137}Ba nuclear magnetic resonance (NMR) spectroscopy. ^{137}Ba NMR spectra for the undeformed reference sample by rotating along a [001], b [110], c [-110] directions, respectively. ^{137}Ba NMR spectra for the deformed sample by rotating along d [001], e [110], and f [-110] directions, respectively. The lower signal-to-noise ratio (SNR) for rotating around the [110] direction (b and e) can be explained by the fact that the gold electrodes were not removed in order to be able to repeat poling, if necessary. In this particular orientation, the presence of the electrodes leads to electric shielding and eddy currents, which cause a considerable loss of intensity. On one hand, when the rotation axis (*y*-axis) is perpendicular to the applied magnetic field B_0 (namely, along the rotation along the [001] direction), the largest vector in the ellipsoids indicates the direction of the spontaneous polarization, aligning with the main component of the EFG tensor[1]. In this specific configuration of the goniometer probe, the green ellipsoid consistently aligns in perpendicular orientation to the magnetic field. Consequently, the position of the corresponding ^{137}Ba NMR signal remains independent of the rotation angle and is consistently located at approximately 478±2 ppm (*c*-domains). Conversely, the relative orientation between the red ellipsoid and the magnetic field, as well as the relative orientation of the blue ellipsoid and the magnetic field, changes with the rotation angle (see a and d). On the other hand, when the rotation axis (*y*-axis) aligns with either the [110] or [-110] direction, the largest vector in the ellipsoids forms a specific angle with the main component of the EFG tensor. As a result, the position of the corresponding ^{137}Ba NMR signal remains unaffected by the rotation angle[2] (see b, e, c, and f). The areas of the signals and their varying dependence on orientation are employed to ascertain the relative proportions of individual domain configurations in the single crystals.

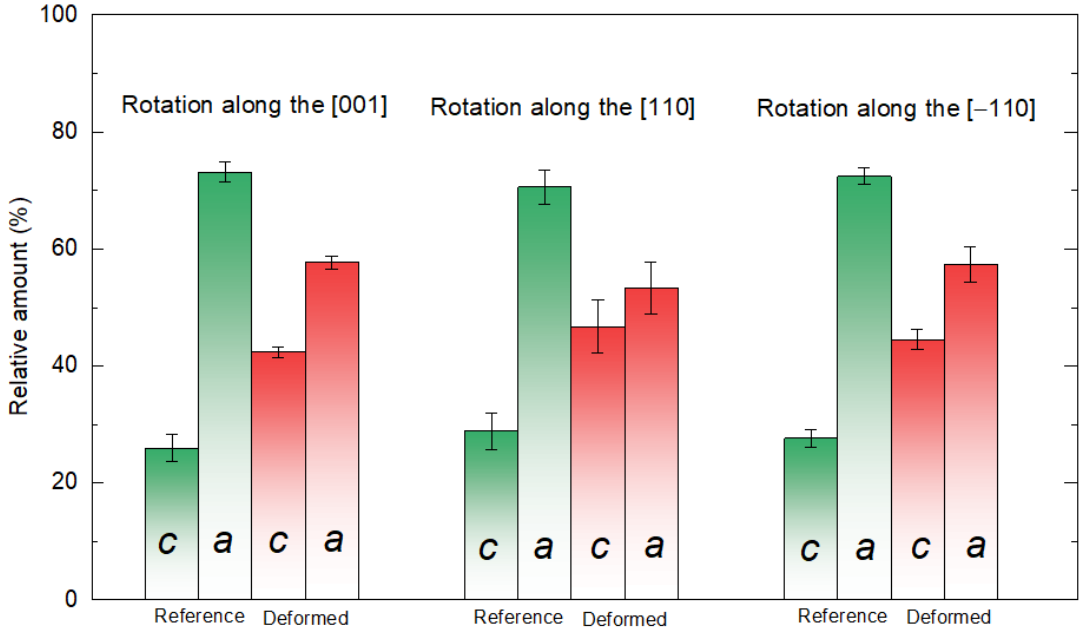

Fig. S4 Relative *a*/*c* domain ratios of both reference and deformed samples by ^{137}Ba nuclear magnetic resonance (NMR) spectroscopy. The average *c*/*a* domain ratios of reference and deformed samples are 38% and 79%, respectively. (In the ideal case where each domain has an equal chance to nucleate, the expected c/a domain ratio would be approximately 33%)

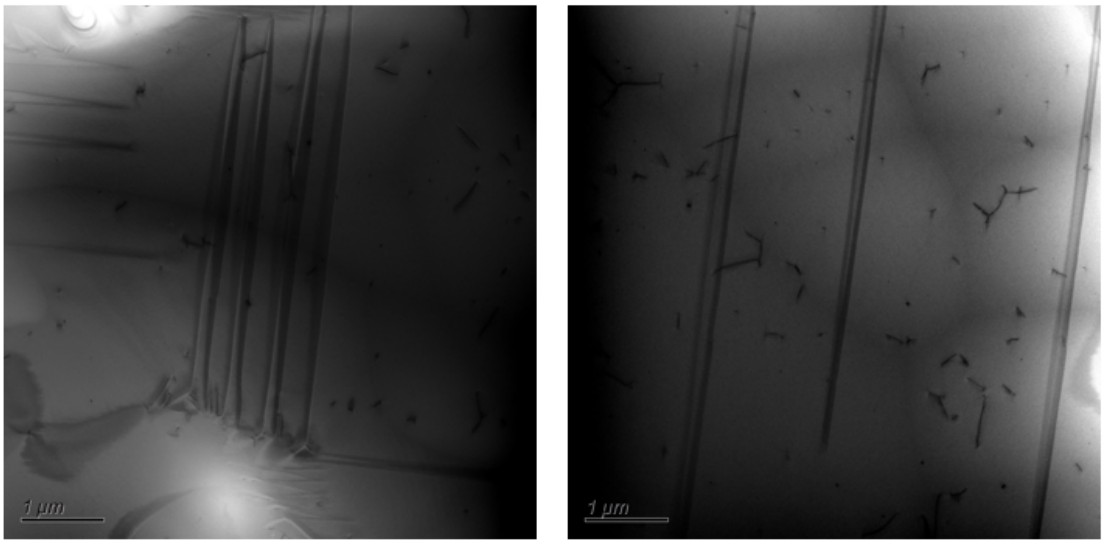

Fig. S5 Dislocations viewed on (001) planes. Representative bright-field TEM images of the deformed $BaTiO_3$ sample. The estimated dislocation density is 1.5×10^{12} m^{-2}.

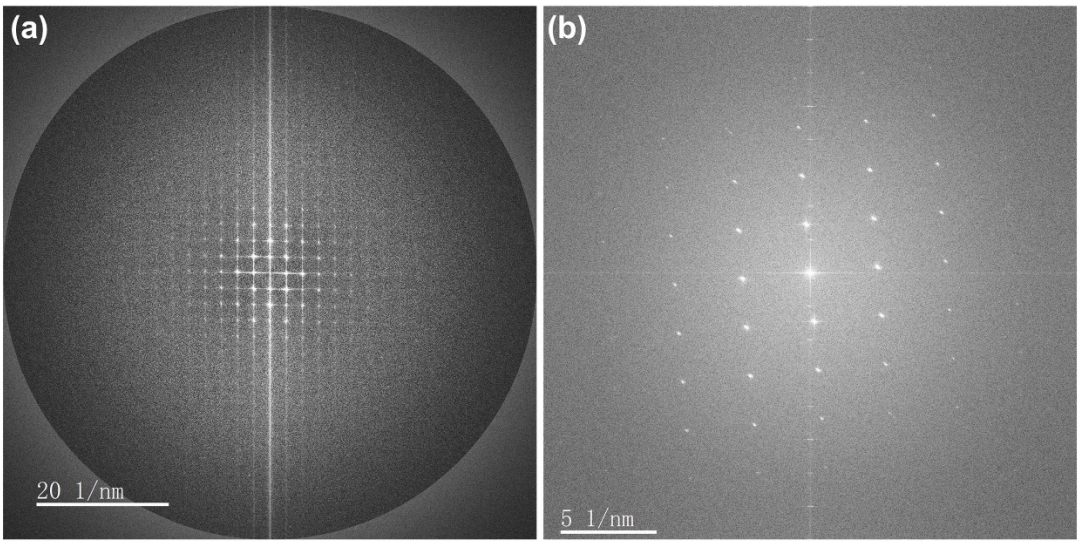

Fig. S6 FFT pattern of the deformed samples. FFT patterns of deformed $BaTiO_3$ single crystal along (001) plane (a) and (110) plane (b).

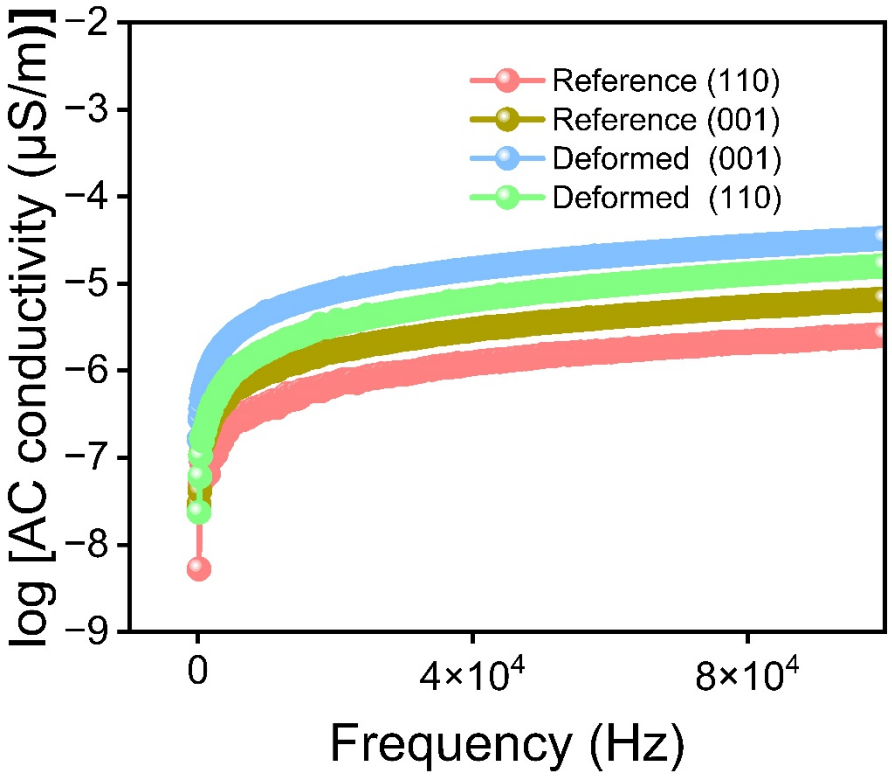

Fig. S7 Conductivity of the deformed and reference samples.

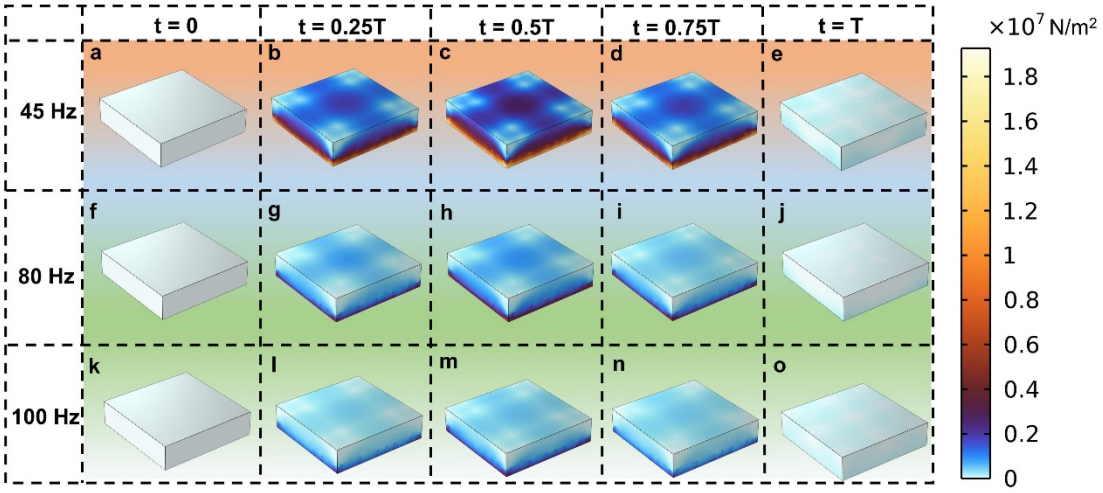

Fig. S8 Stress distribution of $BaTiO_3$ single crystals at different ultrasonic frequencies. The instantaneous stress distribution at t = 0 (a), t = 0.25T (b), t = 0.5T (c), t = 0.75T (d) and t = T (e) with an ultrasonic frequency of 45 Hz. The instantaneous stress distribution at t= 0 (f), t = 0.25T (g), t = 0.5T (h), t = 0.75T (i) and t = T (j) with an ultrasonic frequency of 80 Hz. The instantaneous stress distribution at t = 0 (k), t = 0.25T (l), t = 0.5T (m), t = 0.75T (n) and t = T (o) with an ultrasonic frequency of 100 Hz.

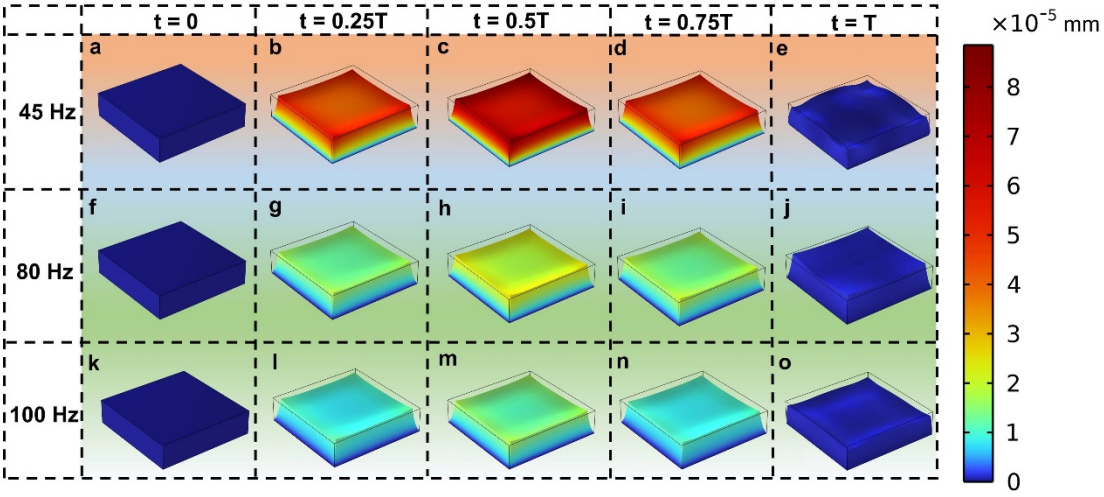

Fig. S9 Deformation of $BaTiO_3$ single crystals at different ultrasonic frequencies. The instantaneous deformation distribution at t = 0 (a), t = 0.25T (b), t = 0.5T (c), t = 0.75T (d), and t = T (e) with an ultrasonic frequency of 45 Hz. The instantaneous deformation distribution at t = 0 (f), t = 0.25T (g), t = 0.5T (h), t = 0.75T (i), and t = T (j) with an ultrasonic frequency of 80 Hz. The instantaneous deformation distribution at t = 0 (k), t = 0.25T (l), t = 0.5T (m), t = 0.75T (n), and t = T (o) with an ultrasonic frequency of 100 Hz.

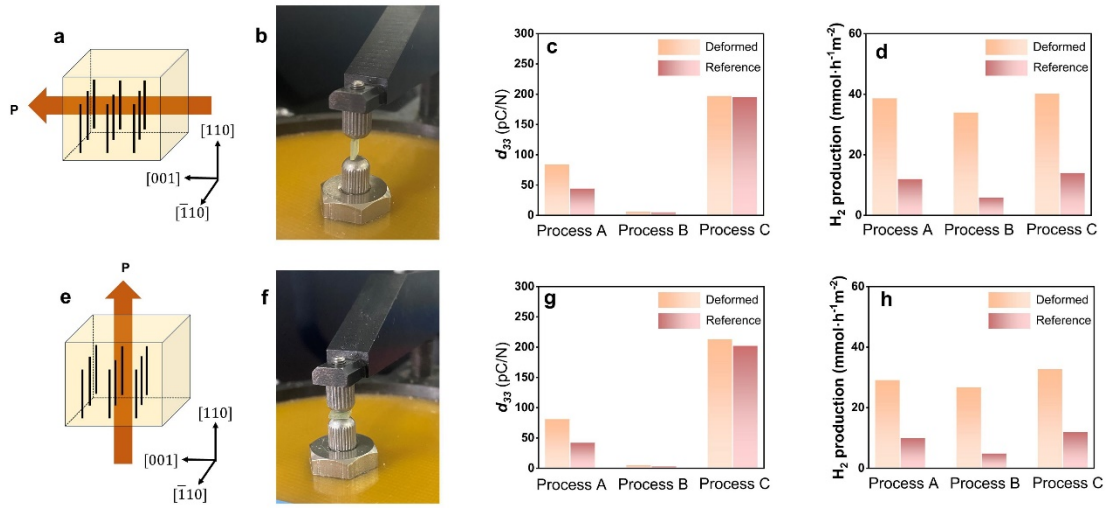

Fig. S10 Polarization effects on piezoelectric coefficient (d_{33}) and hydrogen production. Polarization direction (a), measurement direction of d_{33} (b), d_{33} (c), and hydrogen production (d) of the (001) cut. Polarization direction (e), measurement direction of d_{33} (f), d_{33} (g), and hydrogen production (h) of the (110) cut. Process A refers to no treatment; process B refers to depolarization, and the details of the depolarization process involve heating the sample at a rate of 1°C/min until it reaches 150°C; process C refers to polarization after process B. The polarization process involves placing the sample on a heating platform at 70°C and applying a high voltage of 17 kV. After two hours, the electric field is turned off, and the sample is removed. The polarized samples need to wait for 24 h before conducting a d_{33} test.

For the (001) cut, measurements of d_{33} along its polarization direction yielded results close to zero, consistent with our previous report[3]. However, we still detected a non-zero d_{33} when measuring perpendicular to the polarization direction. In the case of the (110) cut sample, the polarization direction aligned with the measurement direction of d_{33}.

The results indicate that depolarization and repolarization can alter the d_{33} of the samples, affecting hydrogen production to some extent. However, the observed changes in hydrogen production are relatively minor. This suggests that d_{33} measurement is from the global deformation of the sample, while the piezocatalysis is more related to the local strain around the dislocations.

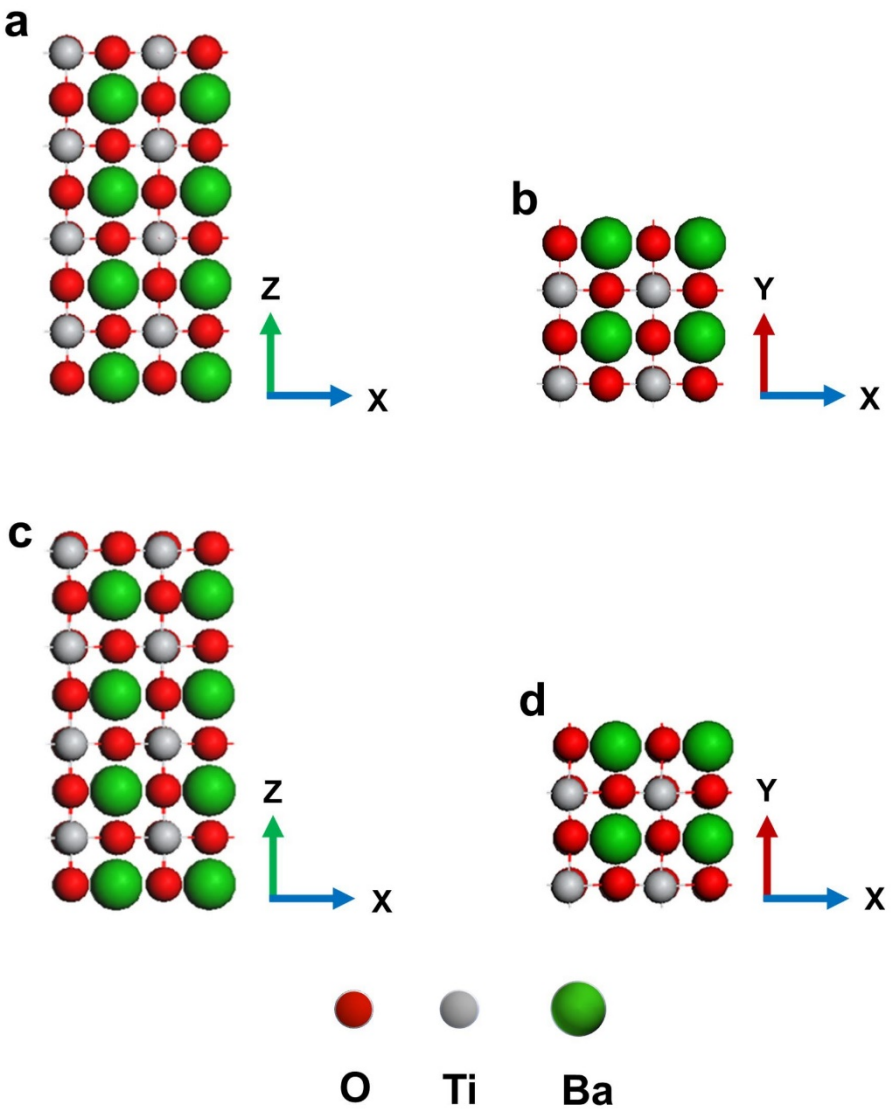

Fig. S11 Snapshots of initiating structure and relaxed models of (001) $BaTiO_3$ slab. a Front view and b top view of the initial models of (001) $BaTiO_3$ slab. c Front view and d top view of the relaxed models of (001) $BaTiO_3$ slab.

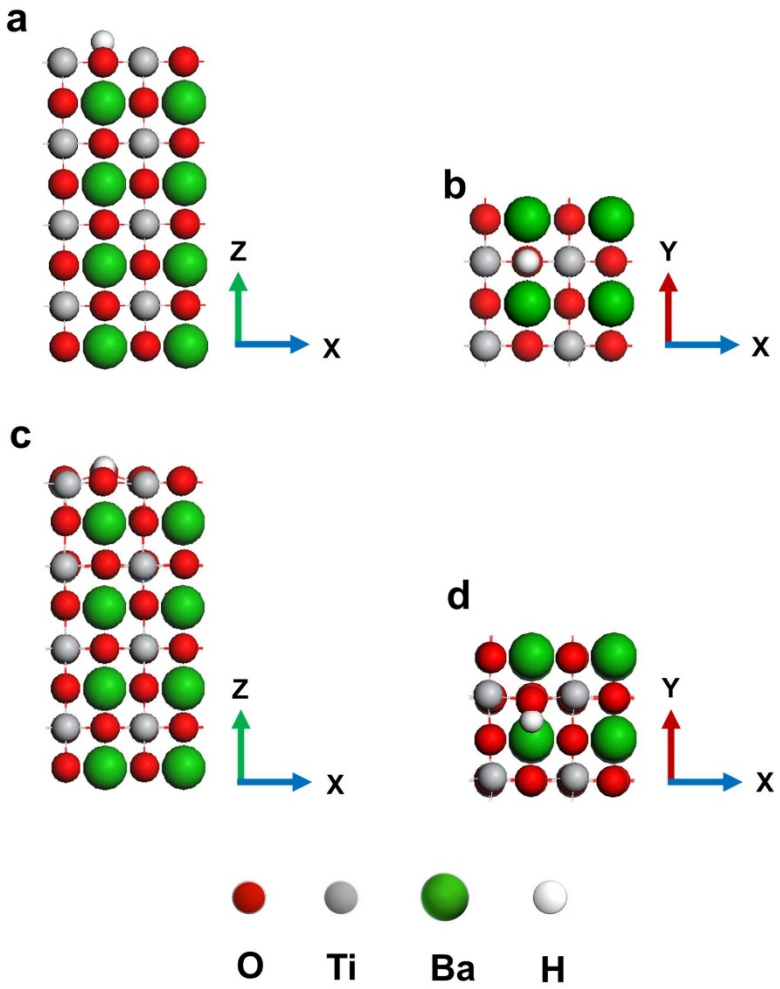

Fig. S12 Snapshots of initiating structure and relaxed models of H* absorbed on the (001) $BaTiO_3$ slab. a Front view and b top view of the initial models of H^* absorbed on the (001) $BaTiO_3$ slab. c Front view and d top view of the relaxed models of H^* absorbed on the (001) $BaTiO_3$ slab.

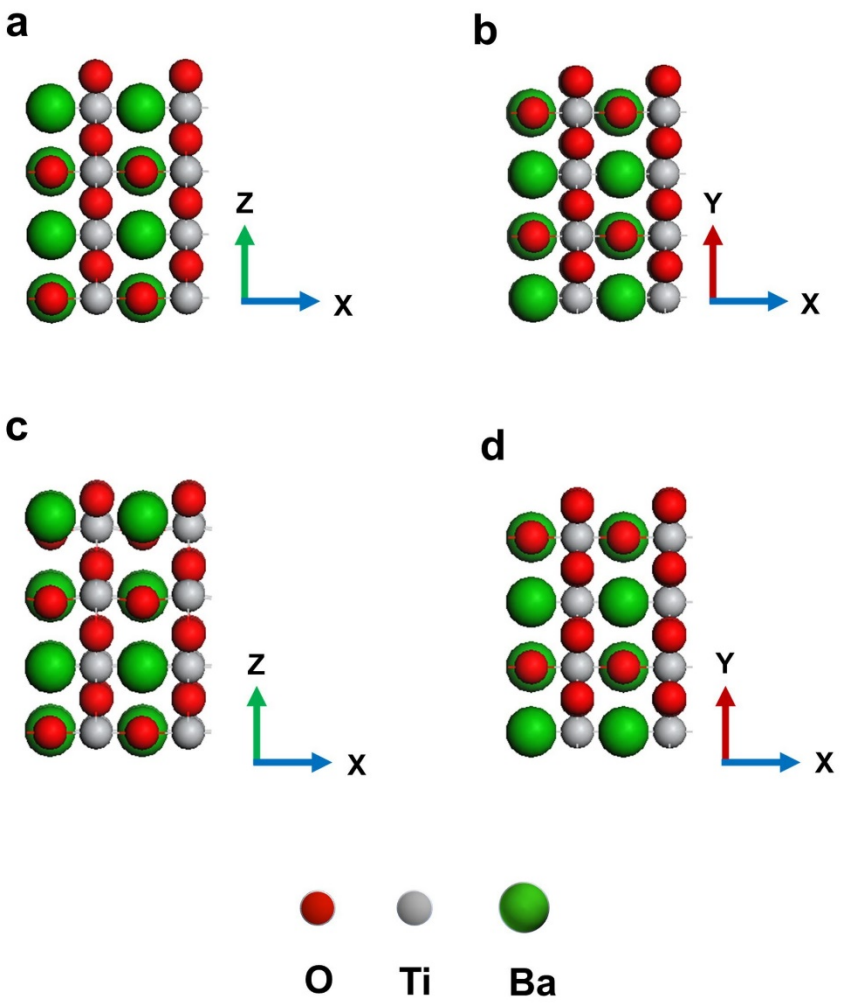

Fig. S13 Snapshots of initiating structure and relaxed models of (110) $BaTiO_3$ slab. a Front view and b top view of the initial models of (110) $BaTiO_3$ slab. c Front view and d top view of the relaxed models of (110) $BaTiO_3$ slab.

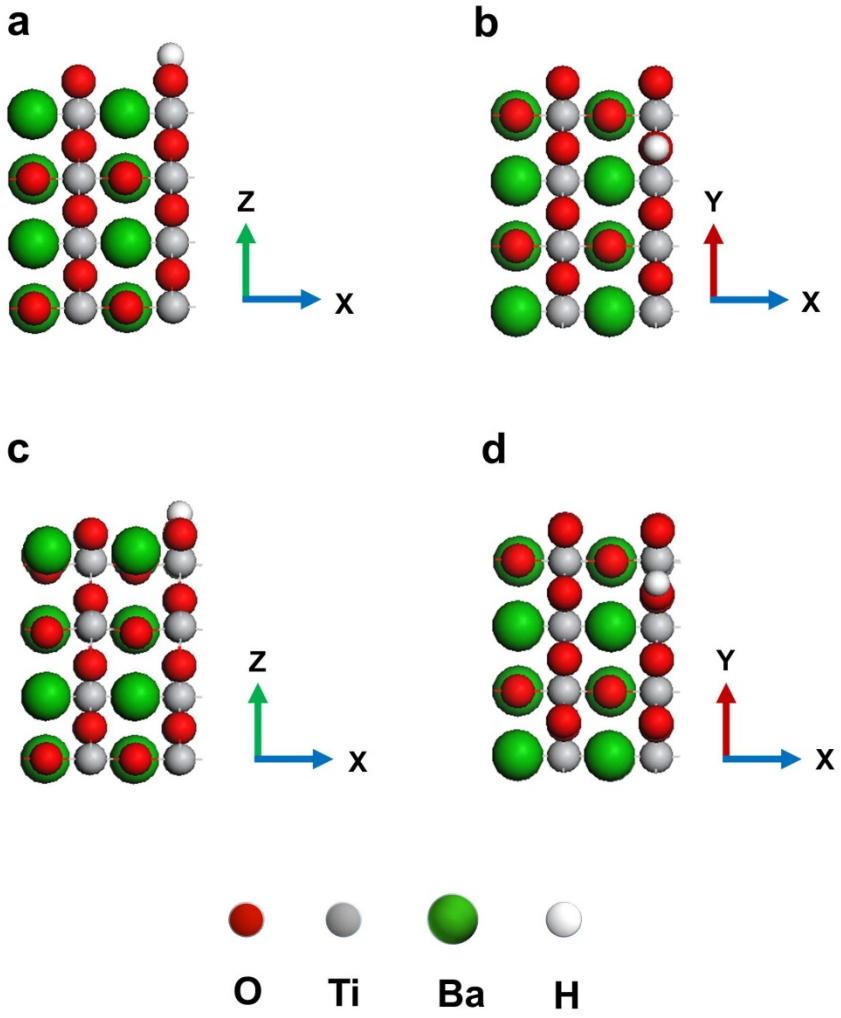

Fig. S14 Snapshots of initiating structure and relaxed models of H* absorbed on the (110) $BaTiO_3$ slab. a Front view and b top view of the initial models of H^* absorbed on the (110) $BaTiO_3$ slab. c Front view and d top view of the relaxed models of H^* absorbed on the (110) $BaTiO_3$ slab.

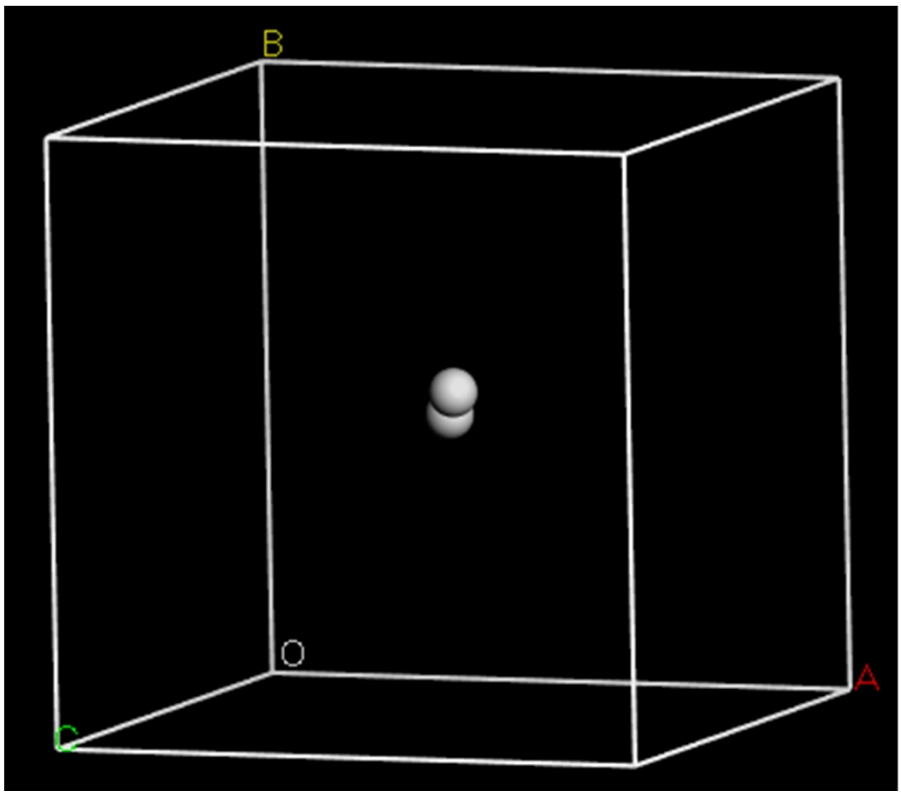

Fig. S15 Model established for calculating the energy of hydrogen gas. The lattice size is 10×10×10 Å.

Table S1. Energy (eV) of (001) $BaTiO_3$ slab and (001) $BaTiO_3$ slab with adsorbed H^* (rounded to two decimal places)

	Reference	2% tensile strain	3% tensile strain
$BaTiO_3$ slab	-63168.52	-63169.14	-63168.67
$BaTiO_3$ slab with H^*	-63185.25	-63185.48	-63185.02

Table S2. Energy (eV) of (110) $BaTiO_3$ slab and (110) $BaTiO_3$ slab with adsorbed H^* (rounded to two decimal places)

	Reference	2% tensile strain	3% tensile strain
$BaTiO_3$ slab	-63142.61	-63143.07	-63142.62
$BaTiO_3$ slab with H^*	-63161.20	-63161.65	-63161.20

References

1. T. Gullion and J. Schaefer, *J. Magn. Reson.*, 1989, **81**, 196-200.
2. M. Höfling, X. D. Zhou, L. M. Riemer, E. Bruder, B. Z. Liu, L. Zhou, P. B. Groszewicz, F. P. Zhuo, B. X. Xu, K. Durst, X. L. Tan, D. Damjanovic, J. Koruza and J. Rödel, *Science*, 2021, **372**, 961.
3. F. P. Zhuo, X. D. Zhou, S. Gao, F. Dietrich, P. B. Groszewicz, L. Fulanovi, P. Breckner, B. X. Xu, H. J. Kleebe, D. Damjanovic and J. Rödel, *Phys. Rev. Lett.*, 2023, **131**, 016801.